Biomaterials 274 (2021) 120899

Contents lists available at ScienceDirect

Biomaterials

journal homepage: www.elsevier.com/locate/biomaterials

Hepatic patch by stacking patient-specific liver progenitor cell sheets formed on multiscale electrospun fibers promotes regenerative therapy for liver injury

Yohan Kim [a,b,1], Young Won Kim [c,1,2], Seung Bum Lee [d,1], Kyojin Kang [a], Sangtae Yoon [a,b], Dongho Choi [a,b,***], Suk-Hee Park [e,**], Jaemin Jeong [a,b,*]

[a] Department of Surgery, Hanyang University College of Medicine, Seoul, 04763, Republic of Korea
[b] HY Indang Center of Regenerative Medicine and Stem Cell Research, Hanyang University, Seoul, 04763, Republic of Korea
[c] Digital Manufacturing Process Group, Korea Institute of Industrial Technology, 113-58 Seohaean-ro, Siheungsi, Gyeonggi-do, 15014, Republic of Korea
[d] Laboratory of Radiation Exposure & Therapeutics, National Radiation Emergency Medical Center, Korea Institute of Radiological & Medical Science, Seoul, 01812, Republic of Korea
[e] School of Mechanical Engineering, Pusan National University, Busan, 46241, Republic of Korea

ARTICLE INFO

Keywords:
Human hepatocytes
Human chemically derived hepatic progenitors
Electrospun fiber scaffold
Hepatic cell sheet and hepatic patch

ABSTRACT

Recently, use of cell sheets with bio-applicable fabrication materials for transplantation has been an attractive approach for the treatment of patients with liver failure. However, renewable and scalable cell sources for engineered tissue patches remain limited. We previously reported a new type of proliferating bipotent human chemically derived hepatic progenitor cells (hCdHs) developed by small molecule-mediated reprogramming. Here, we developed a patient-specific hepatic cell sheet constructed from liver biopsy-derived hCdHs on a multiscale fibrous scaffold by combining electrospinning and three-dimensional printing. Analysis of biomaterial composition revealed that the high-density electrospun sheet was superior in increasing the functional properties of hCdHs. Furthermore, the hepatic patch assembled by multilayer stacking with alternate cell sheets of hCdHs and human umbilical vein endothelial cells (HUVECs) recapitulated a liver tissue-like structure, with histological and morphological shape and size similar to those of primary human hepatocytes, and exhibited a significant increase in hepatic functions such as albumin secretion and activity of cytochrome P450 during *in vitro* hepatic differentiation compared with that in hCdH cells cultured in a two-dimensional monolayer. Interestingly, in the hepatic patch, the induction of functional hepatocytes was associated with both the electrospun fibrous-facilitated oncostatin M signaling and selective activation of AKT signaling by HUVECs. Notably, upon transplantation into a mouse model of therapeutic liver repopulation, the hepatic patch effectively repopulated the damaged parenchyma and induced the restoration of liver function with healthy morphology in the lobe and an improved survival rate (>70%) in mice. Overall, these results suggested that liver biopsy-derived hCdHs can be an efficient alternative source for developing hepatic cell sheets and patches with potential clinical applications in tissue engineering to advance liver regeneration.

1. Introduction

Hepatocyte transplantation is one of the most available approaches for the treatment of patients with liver failure induced by alcohol consumption, hepatotoxic drugs, or viral infections. However, the use of human hepatocytes has been hindered by the shortage of donor tissue, limited numbers of cells suitable for transplantation, and low efficiency of engraftment in diseased livers [1–3]. In addition, mature human

* Corresponding author. Department of Surgery, Hanyang University College of Medicine, Seoul, 04763, Republic of Korea.
** Corresponding author.
*** Corresponding author. Department of Surgery, Hanyang University College of Medicine, Seoul, 04763, Republic of Korea.
E-mail addresses: crane87@hanyang.ac.kr (D. Choi), selome815@pusan.ac.kr (S.-H. Park), jmj1103@gmail.com (J. Jeong).
[1] These authors contributed equally to this study as co-first authors.
[2] Present address : School of Mechanical Engineering, Purdue University, West Lafayette, IN 47907, USA

https://doi.org/10.1016/j.biomaterials.2021.120899
Received 1 September 2020; Received in revised form 10 May 2021; Accepted 15 May 2021
Available online 18 May 2021

hepatocytes are difficult to maintain and proliferate *in vitro* owing to the loss their proliferative potential during culture. Based on the strategy of cell fate conversion by small molecules, we have recently succeeded in generating human chemically derived hepatic progenitor cells (hCdHs) with the potential for high proliferation and bi-lineage differentiation, such as hepatocyte and biliary epithelial cells, both *in vitro* and *in vivo* [4]. Upon implantation *in vivo*, the hCdHs acquired mature hepatocyte properties and secreted human albumin, implying that hCdHs possess a remarkable hepatocyte-forming potential *in vivo*.

In recent years, cell sheet-based tissue engineering has attracted much attention as an alternative approach in cell transplantation therapy [5,6] because it can be used to enhance the engraftment efficiency without any loss of transplanted cells. A previous study showed that the function and therapeutic effects of hepatic cell sheets after transplantation were higher than those of direct cell infusion [7]. The development of liver tissue-like phenotype and function was facilitated by utilizing human umbilical vein endothelial cells (HUVECs) and stacking them in a layer-by-layer manner [8], but these biomimetic structures comprised double layers with each cell sheet rather than multilayers mimicking the structure of an *in vivo* liver (Scheme 1). Furthermore, hepatic sheets for transplantation have been developed using hepatocyte-like cells derived from various stem cells such as pluripotent stem cells (PSCs) and mesenchymal stem cells (MSCs) [9,10]. Because hCdHs retain a superior capacity for hepatic functionality to other stem cells, we hypothesize that hCdH-derived hepatocytes (hCdH-Heps) are a potential cell source for hepatic cell sheet transplantation. However, the feasibility and therapeutic effects of cell sheet transplantation of human hepatic progenitor cells on the liver surface are yet to be elucidated.

Most technical approaches in cell sheet-based tissue engineering are based on cells seeded on a scaffold to mimic the microenvironment of the extracellular matrix (ECM). Among both natural and synthetic materials used to develop various scaffolds, polycaprolactone (PCL) scaffold material is one of the most biocompatible formulations to generate fibrous scaffolds as ECM substitutes [6,11]. Multiscale PCL electrospun fiber mats can be produced by electrospinning and three-dimensional (3D) printing, which is widely used to fabricate tissue engineering scaffolds [12,13]. In the context of cellular functionality, an electrospun fibrous scaffold with an ECM-like structure modulates physiological functions by activating various intracellular signaling pathways related to cellular processes such as cell mobility, proliferation, and differentiation [13,14]. However, the cellular mechanism underlying electrospun fibrous scaffold-supported hepatic differentiation from hepatic progenitor cells for engineering hepatic cell sheets is not completely elucidated.

Oncostatin M (OSM) is a member of the interleukin-6 (IL-6) cytokine family, which includes interleukin-6, interleukin-11, and leukemia inhibitory factor (LIF). The OSM signaling pathway involves two different heterodimeric receptors that share gp130 (a common subunit receptor for ligands of the IL-6 family) and either LIF receptor β (LIFRβ) or OSM receptor β (OSMRβ), which is expressed in the hepatocytes of normal livers [15]. Functionally, OSM critically regulates processes such as liver development involving the maturation of fetal hepatocytes, hematopoiesis, and angiogenesis through the Janus kinase/signal transducer and activator of transcription (JAK/STAT), PI-3 kinase-Akt (PI3K/AKT), and the mitogen-activated protein kinase (MAPK) pathways [16]. In addition to its role in liver development, OSM is also involved in regulating inflammatory responses in several diseases affecting different organs and tissues. Furthermore, the expression of pro-inflammatory cytokines such as IL6 and TNF-α in various cell types can be regulated by nanofibrous scaffolds [17,18], suggesting the existence of cross-talk between OSM and nanofibers during liver development, especially during hepatic maturation.

In this study, to determine whether patient liver-derived reprogrammed hepatic progenitor cells can be a new cell source for hepatic cell sheet transplantation, we generated patient-specific hCdHs from tissues obtained by liver biopsy from the surgical specimen and developed a hepatic cell sheet and patch for transplantation by seeding either hCdHs or HUVECs into electrospun fibrous scaffolds in a layer-by-layer manner (Scheme 1). Functional analysis revealed that the hepatic patch synthesized using hCdHs recapitulated a liver tissue-like structure and promoted liver regeneration in a hepatic injury mouse model by acquiring functional hepatocyte-like cells associated with OSM-dependent and OSM-independent signaling pathways. Therefore, patient-specific hCdHs may be a novel source to develop hepatic cell sheets/patches for application in personalized tissue engineering and cell sheet-based regenerative medicine.

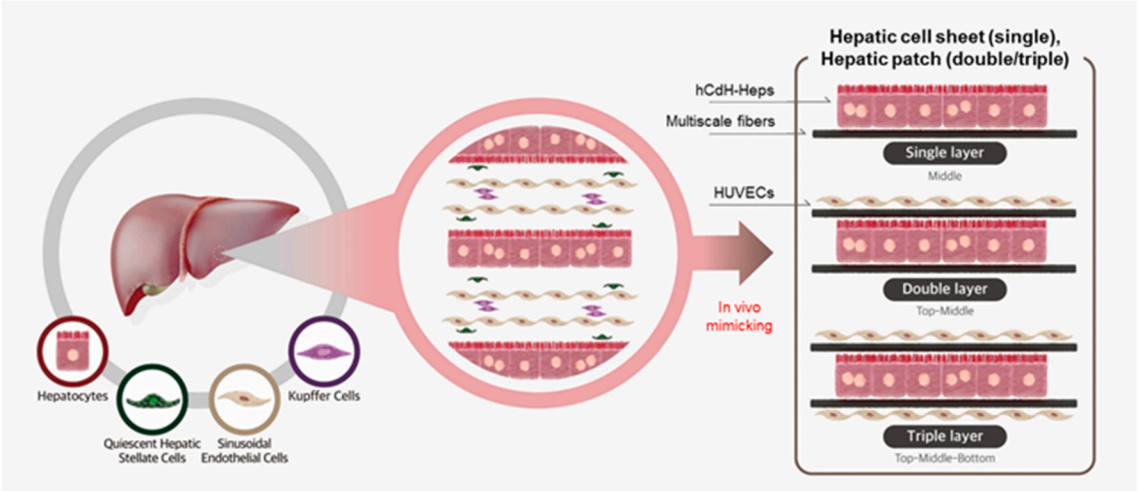

Scheme 1. Schematic illustration of *in vivo* liver-mimicking hepatic cell sheets and patch. To generate the hepatic cell sheet and patch, hCdHs or HUVECs were seeded onto each electrospun fibrous sheet as indicated, and functional hepatocytes from the hCdHs (hCdH-Heps) were induced under *in vitro* hepatic differentiation conditions. Single-layers had hepatic cell sheets containing hCdH-Heps on the fibrous sheet, while multilayers (double and triple) had a hepatic patch containing a hepatic cell sheet and a HUVEC sheet with differential arrangement of cells, respectively. hCdHs: human chemically derived hepatic progenitor cells, hCdH-Heps: hCdHs-derived hepatocytes, HUVECs: human umbilical vein endothelial cells.

2. Materials and methods

2.1. Fabrication of edge-framed electrospun sheets

For electrospinning, the polymer solutions were prepared by dissolving PCL granules (MW 80,000; Sigma-Aldrich, St. Louis, MO, USA) in a mixed solvent of dichloromethane and dimethylformamide at 3:1 (v/v). The solution concentration was 14% (w/v). PCL solutions were infused through a blunt-tip metal needle with an inner diameter of 250 μm at a feed rate of 60 μm/min. The spinning needle was connected to a DC power supply, and a high voltage of 20 kV was applied. The distance from the needle tip to the ground collector was 180 mm. The electrospinning times were set as 30 and 180 s to determine the optimal fiber density of the scaffolds. The as-spun fiber sheets were edge-framed by the fused PCL framework structures, which were printed using a customized 3D printing machine that used material extrusion. Before printing, a filament-form feedstock (1.7-mm diameter) was prepared from the PCL granules using a custom-made extrusion machine. The prepared filaments were printed through a hot nozzle with an inner diameter of 0.4 mm at a heating temperature of 100 °C.

2.2. Isolation of human primary hepatocytes (hPHs)

This study was approved by the Institutional Review Board of Hanyang University, Seoul, Republic of Korea (HYI-16-229-3). Liver tissues were obtained from the surgical specimen with consent from a donor who visited Hanyang University Medical Center (Table S1). hPHs were isolated by a two-step collagenase perfusion method as previously described [19]. Biopsied livers were incubated with collagenase for 30 min at 37 °C. Then, hPHs were isolated by Percoll (Sigma-Aldrich) gradient centrifugation.

2.3. Cell culture and reprogramming into hepatic progenitors

First, the hPHs (1×10^5 cells/well) were seeded onto collagen-coated six-well culture dishes (Advanced BioMatrix, San Diego, CA, USA) in basal medium, DMEM/F-12 (Gibco, Gaithersburg, MD, USA) supplemented with 1% fetal bovine serum (Gibco), 1% insulin-transferrin-selenium (Gibco), 0.1 μM dexamethasone (Sigma-Aldrich), 50 μM 2-mercaptoethanol (Sigma-Aldrich), 10 mM nicotinamide, 20 ng/mL epidermal growth factor (Peprotech, Cranbury, NJ, USA), and 1% penicillin/streptomycin (Gibco). After overnight incubation at 37 °C with 5% CO_2, the basal medium was replaced with a reprogramming medium comprising a basal medium supplemented with 20 ng/mL of hepatocyte growth factor (HGF, Peprotech), 4 μM A83-01 (Gibco), and 3 μM CHIR99021 (STEMCELL Technologies, Cambridge, MA, USA), hereafter termed HAC [4]. The reprogramming medium was changed every couple of days, and each split was performed at a 1:3 ratio. HUVECs were cultured in Endothelial Cell Growth Basal Medium-Plus (EBM™-Plus, Lonza, Basel, Switzerland) with a Plus SingleQuot™ Kit and growth supplements (EGM™-Plus Endothelial Cell Growth Medium). The medium was changed every couple of days, and each split was performed at a 1:3 ratio.

2.4. Electrospun fibrous sheet stacking and hepatic differentiation studies

The hCdHs and HUVECs were both plated on electrospun fibrous sheets at 1×10^5 cells and cultured in the reprogramming medium and EGM (Lonza), respectively. After 3 days of incubation, the sheets were stacked according to the designed formation in the reprogramming medium and EGM at a 1:1 ratio for stable proliferation of both cells. Before stacking, collagen gel solution (Advanced BioMatrix) was coated on the cell-cultured sheets and cured at 37 °C with 5% CO_2 to obtain a structurally robust stacking assembly. A single layer was formed when only hCdHs were seeded, double layer when hCdHs and HUVECs were seeded, and triple layer when HUVECs, hCdHs, and HUVECs were seeded (Scheme 1). As a two-dimensional (2D) control, hCdHs and HUVECs were seeded onto six-well plates at 1×10^5 cells/well, respectively. After overnight incubation, the medium was replaced with a hepatic differentiation medium comprising the reprogramming medium (maintained with HAC) supplemented with 20 ng/mL OSM (R&D Systems, Minneapolis, MN, USA) and 10 μM dexamethasone for 14 days. The hepatic differentiation medium was changed every 2 days.

2.5. Lentivirus production

mCherry lentivirus was packaged by co-transfection with psPAX2 lentiviral packaging plasmids and pCMV-VSV-G plasmids in human embryonic kidney 293 T cells. Culture supernatants containing the viruses were harvested 72 h after transfection, filtered, and stored at −80 °C. The titer of the virus preparations was $<10^7$ IFU/mL, as determined by a Lenti-X p24 rapid titer kit (Takara Bio, Inc. Kusatsu, Shiga, Japan).

2.6. Isolation of mRNA and quantitative reverse-transcription polymerase chain reaction (RT-qPCR)

Total RNA was extracted from samples using TRIzol reagent (Gibco). Then, cDNA samples were synthesized using a Transcriptor First Strand cDNA Synthesis Kit (Roche, Basel, Switzerland), and real-time PCR was performed with qPCR PreMix (Dyne Bio, Seongnam-si, Gyeonggi-do) using a CFX Connect Real-Time PCR Detection system (Bio-Rad, Hercules, California, USA). All reactions were performed in triplicate. Primer sequences are listed in Table S2.

2.7. Immunofluorescence staining

Antibodies used in this study are listed in Table S3. Staining was performed according to the manufacturer's instructions. Nuclei were counterstained with Hoechst 33342 (1:10000, Molecular Probes, Eugene, OR, USA). Fluorescently stained cells were viewed under a TCS SP5 confocal microscope (Leica, Wetzlar, Hesse, Germany).

2.8. Human albumin assay

The presence of human albumin was determined in the culture medium using a Human Albumin Enzyme-Linked Immunosorbent Assay (ELISA) Kit (Bethyl Laboratories, Montgomery, TX, USA) according to the manufacturer's recommendations. The culture medium from the hCdH-Heps was subjected to a hepatocyte differentiation protocol for 14 days (measured in triplicate). Mouse serum was collected after administration of diphtheria toxin (DT) only (DT-only group) and transplantation of the hCdHs and hepatic patch (transplanted group).

2.9. Cytochrome P450 (CYP) activity assay

To measure CYP1A2, CYP2C9, and CYP3A4 activity, the hCdHs, hCdH-Heps, and hPHs were treated with 100 μM omeprazole (to induce the CYP1A2 activity) and 25 μM rifampicin (to induce the CYP2C9 and CYP3A4) for 4 days, respectively. CYP activity was determined using the P450-Glo Assay (Promega, Madison, WI, USA) according to the manufacturer's recommendations. Each experiment was performed in triplicate.

2.10. Detection of human OSM and vascular endothelial growth factor (VEGF)

To detect human OSM and VEGF, conditioned media of the 2D control, sheet, and patch with hCdHs were collected after hepatic differentiation. Human OSM and VEGF were measured using the Human OSM ELISA Kit (Abcam, Cambridge, UK) and Human VEGF Quantikine ELISA Kit (R&D Systems), respectively, according to the manufacturer's

recommendations. Each experiment was performed in triplicate.

2.11. Scanning electron microscopy (SEM)

The ultrastructure of the electrospun fibers and cultured cells was visualized using SEM as described in a previous study [20]. The cell-laden scaffolds were washed three times with phosphate-buffered saline and fixed for 30 min in 5% glutaraldehyde solution containing 0.1 M sodium cacodylate (Sigma) and 0.1 M sucrose (Sigma). After washing with distilled water for 5 min, the samples were slowly dehydrated by serial incubation in 50%, 60%, 70%, 80%, 90%, and 100% ethanol solutions for 5 min each and then treated with hexamethyldisilazane (J. T. Baker, Phillipsburg, NJ, USA) for 15 min. When completely dried, the samples were sputtered with Pt until a 20-nm-thick coating was obtained. The samples were then imaged via SEM (S-4800; Hitachi, Japan).

2.12. Western blotting

Cells were lysed in a buffer containing 50 mM Tris-HCl (pH 7.4), 5 mM EDTA, 150 mM NaCl, 1% Triton X-100, and a protease inhibitor mixture. Equal amount of protein (20 μg) was separated by 8% sodium dodecyl sulfate-polyacrylamide gel electrophoresis and then electrotransferred to Immobilon membranes (Millipore, Bedford, MA), which were subsequently blotted using the indicated antibodies and visualized using chemiluminescence (Amersham ECL, Marlborough, MA, USA).

2.13. Animal experiments

Alb-TRECK/SCID mice (kindly gifted by Dr. Taniguchi) were housed and cared for under specific-pathogen-free conditions in accordance with the HYU Industry-University Cooperation Foundation regulations (2019–0149). One day before transplantation, the mice were injected with 1.5 μg/kg of DT to induce liver damage. For hepatic patch transplantation, the liver surfaces of 7 mice were exposed and the hepatic patch, after being washed with DMEM/F-12 media, was carefully placed on the liver surface and sutured; these operations were repeated. For sham operation, the liver surfaces of 7 mice were exposed and the just washed with DMEM/F-12 media. For the detection of human albumin using ELISA, mouse serum was collected. Serum samples were diluted at a ratio of 1:4 to determine the ELISA. The levels of hepatic damage and function markers alanine aminotransferase (ALT), total bilirubin, ALB, and alkaline phosphatase (ALP) in the serum of transplanted mice were measured using a biochemical analyzer (FUJI DRI-CHEM, NX700i, Fuji film).

2.14. Statistical analysis

Quantitative data are presented as mean ± standard deviation with inferential statistics (p-values). Statistical significance was evaluated by two-tailed *t*-tests with significance set at $*p < 0.05$, $**p < 0.01$, and $***p < 0.001$.

Supporting Information

Supporting Information is available online or from the authors.

3. Results and discussion

3.1. Synthesis and characterization of patient-specific hCdHs from biopsied liver tissue

To produce functional hepatocyte-like cells that are stably cultured *in vitro*, many studies have been conducted on alternative cell sources, including embryonic stem cells (ESCs) [21,22], induced PSCs (iPSCs) [23,24], MSCs [25,26], and directly converted hepatocyte-like cells [27,28]. However, the use of ESCs faces ethical issues, MSCs rapidly lose their differentiation ability *in vitro* and most of stem cells including iPSCs are associated with a risk of tumorigenesis [29–32]. Previously, our research group developed hCdHs that could stably proliferate and differentiate into functional hepatocyte-like cells (hCdH-Heps) *in vitro* [4]. In the present study, to synthesize hCdHs, hPHs were harvested from the tissues of a biopsied liver (Table S1). Liver biopsy can be performed within few hours, and without major complications in the real world [33]. The hPHs isolated through liver biopsy were rapidly differentiated to proliferating hCdHs in the reprogramming medium after 7 days by an approximate doubling time of 35.2 ± 0.6 h (Fig. 1A, S1A and S1B). The hCdHs maintained the expression of progenitor-specific markers for more than 10 passages (Figure S1C and S1D). Then, the hCdHs effectively differentiated to hepatocyte-like cells 2 weeks later in the hepatic differentiation medium (Fig. 1A). To evaluate the characteristics of the hCdHs and hCdH-Heps, the expression levels of hepatic stem cell and mature hepatocyte-specific markers were determined by RT-qPCR and immunocytochemistry (Fig. 1B–E). The expression levels of hepatic stem cell marker genes (*CK19*, *CD44*, *EpCAM*, *CD90*, and *SOX9*) and proteins (AFP, CK19, and SOX9) were increased in the hCdHs (Fig. 1B and C), whereas those of mature hepatocyte marker genes (*ALBUMIN*, *ASGR1*, *HNF4α*, *MRP2*, and *AAT*) and proteins (ALBUMIN, HNF4α, CK18, and CYP3A4) were increased in the hCdH-Heps (Fig. 1D and E). These results indicated that patient-specific hCdHs could be easily generated from a biopsied liver and maintained in a long-term culture with rapid proliferation and hepatic differentiation potential. Owing to these characteristics, the use of hCdHs may contribute to improve the result of cell-based therapy by generating a large number of cells for clinical applications.

3.2. Fabrication of edge-framed electrospun sheet for multilayer composition and optimization of fiber density in scaffolds for developing functional hepatic sheets of hCdHs

To obtain a histologically similar structure to that observed *in vivo*, we mimicked the liver structure by stacking fibrous electrospun sheets. The base fibrous sheet scaffolds were fabricated by a combination of electrospinning and 3D printing processes, as shown in Fig. 2A. The generated scaffolds comprised an electrospun fiber mat and a 3D printed framework, which provided a foundation for cell adhesion-based functionality and the structural stability of an overall sheet, respectively. Electrospun fibers exhibit tremendous potential for mimicking the microscale organization of native ECM structures, thereby providing a variety of topographic effects regulating the functions of cell adhesion, proliferation, and differentiation [34–36]. In a previous study, the nanofibrous architecture of liver ECM was confirmed using decellularized liver tissues [37]. Typically, the fibril diameters of native ECM are known to range from several nanometers to hundreds of nanometers [38,39]. However, considering practical tissue engineering applications, such ultrafine architecture, characterized by small pores and low permeability, can cause some adverse effects such as obstructive perfusion and inhibition of cell–cell interactions. Typically, the diameters of electrospun fibers are determined by the solution concentration. It is more difficult to break the surface tension of the polymer solution, which is considered a trigger to form fine jets, at high concentrations than at low concentrations. Thus, high concentration solutions generally cause larger fiber diameters with more deviations. Fig. 2B shows the fiber morphologies and distribution of fiber diameters, which ranged from approximately 500 nm to 2.5 μm. This hybrid microstructure, which involved both nanometer- and micrometer-scale features, was expected to provide the scaffold functionalities of nanotopographic effects without deterioration of mass transport conditions for perfusion, which will be addressed in the following sections. After obtaining a fibrous sheet by electrospinning, a framework structure was printed on the edge of the as-spun sheet using an extrusion material-type custom-made 3D printer. To construct the hepatic patch in a

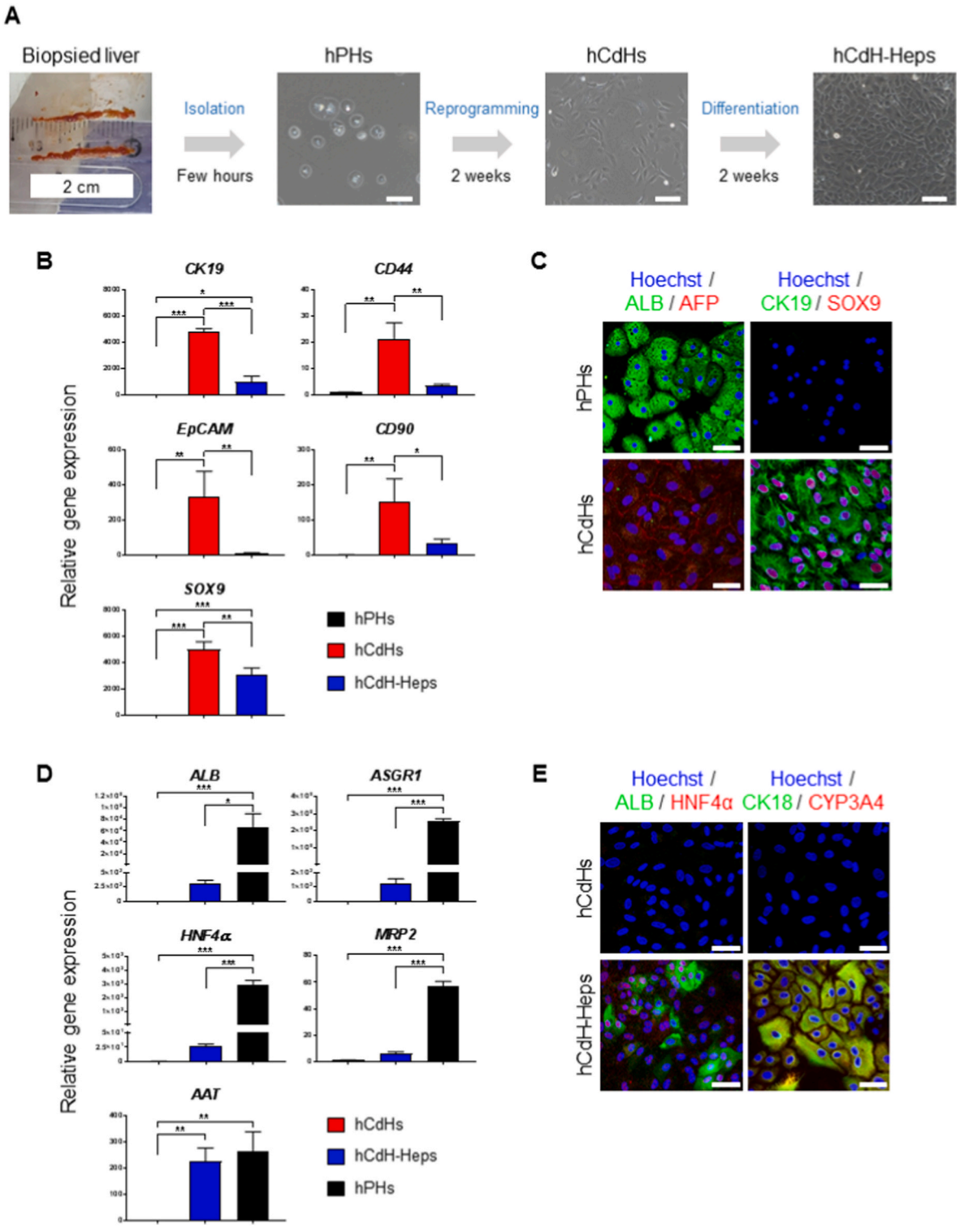

Fig. 1. Generation and characterization of patient-specific hCdHs derived from biopsied human liver. (A) Two-centimeter liver tissue strips were harvested from a patient's liver by a biopsy, and the hPHs were isolated by collagenase. The hPHs isolated from the biopsied liver tissue were then reprogrammed into hCdHs with HAC for 2 weeks. The hCdHs differentiated into hepatocyte-like cells (hCdH-Heps) in the hepatic differentiation medium for 2 weeks. Scale bars, 100 μm. (B) The expression of hepatic progenitor cell markers determined by RT-qPCR. *GAPDH* was used as an internal control for RT-qPCR. Data are means ± SDs (n = 3). Data were analyzed by one-way ANOVA with post-hoc (Tukey). $*p < 0.05$, $**p < 0.01$ and $***p < 0.001$. (C) Immunostaining with hepatic progenitor marker proteins ALBUMIN (green)/AFP (red) and CK19 (green)/SOX9 (red). Nuclei were counterstained with Hoechst 33342 (blue). Scale bars, 50 μm. (D) The mature hepatocyte marker gene expressions determined by qRT-PCR. *GAPDH* was used as an internal control for RT-qPCR. Data are means ± SDs (n = 3). Data were analyzed by one-way ANOVA with post-hoc (Tukey). $*p < 0.05$, $**p < 0.01$ and $***p < 0.001$. (E) Immunostaining with mature hepatocyte marker proteins ALBUMIN (green)/HNF4α (red) and CK18 (green)/CYP3A4 (red). Nuclei were counterstained with Hoechst 33342 (blue). Scale bars, 50 μm hCdHs, human chemically derived hepatic progenitors; hPHs, human primary hepatocytes; RT-qPCR, quantitative reverse transcription PCR; HAC, reprogramming medium.

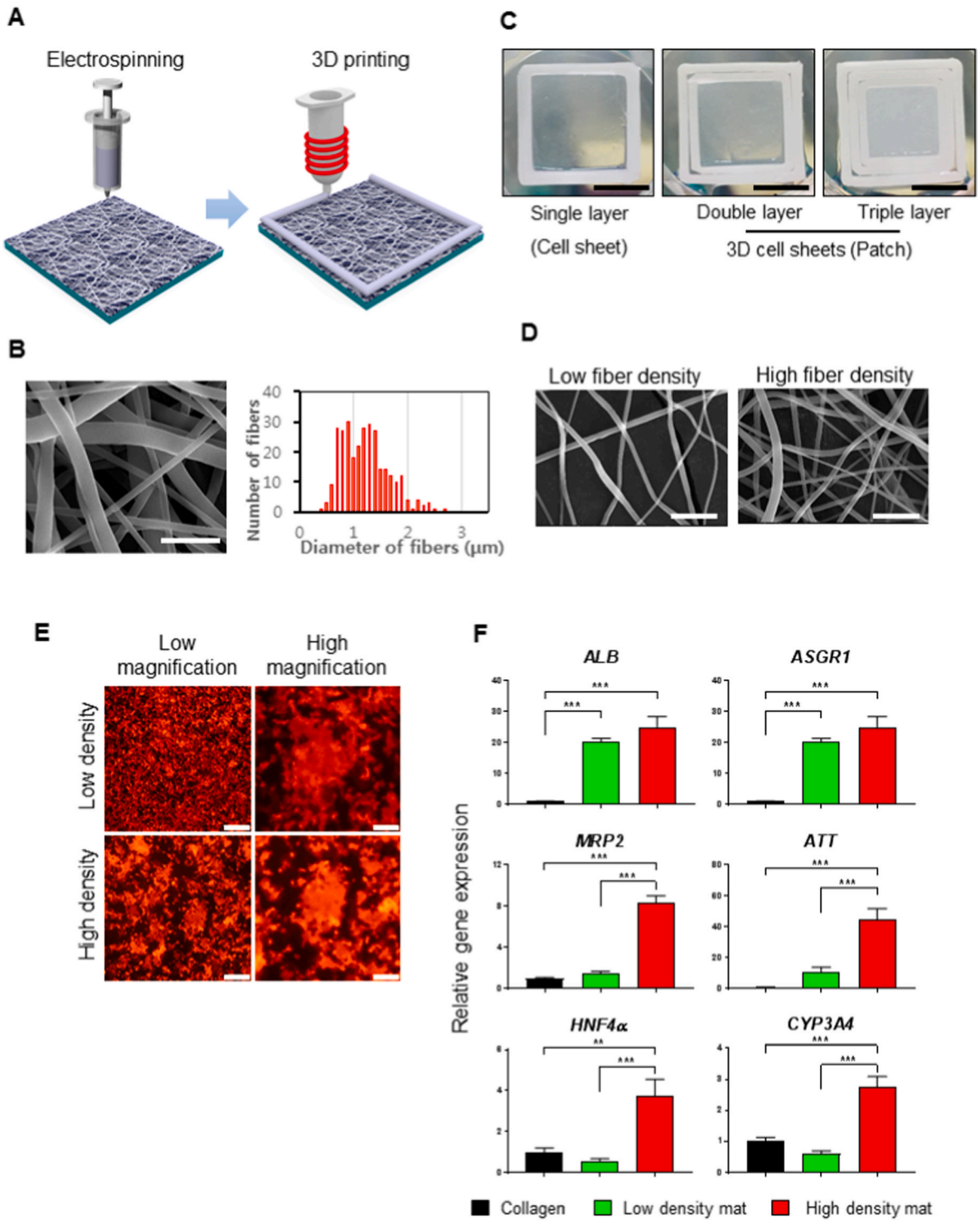

Fig. 2. Manufacturing of edge-framed fibrous sheets for multilayer stacking and optimization of functional hepatocytes on the hepatic cell sheet with different fiber densities. (A) Two-step procedures of electrospinning and edge-framing 3D printing. (B) SEM image of a fibrous scaffold electrospun with 14% (w/v) PCL solution and the resulting distribution of fiber diameters. The scale bar is 5 μm. The 300 fibers were randomly selected from the SEM images and measured for the diameter analysis by using Image J (NIH, USA) software. (C) Multilayer stacking assembly using the three edge-framed fiber scaffolds. The scale bar is 10 mm. (D) SEM images of two types of scaffolds with low and high fiber densities, fabricated by electrospinning for 30 s and 180 s, respectively. Scale bars are 10 μm. (E) Morphological observation of hCdH-Heps cultured on the low- and the high-density fiber scaffolds. Scale bars, 500 μm (low magnification) and 100 μm (high magnification). (F) Relative gene expression levels of mature hepatocyte-specific markers, including *ALB, ASGR1, HNF4A, MRP2, AAT* and *CYP3A4* in hCdH-Heps cultured without or with electrospun fiber sheets, as measured by RT-qPCR. *GAPDH* was used as an internal control. Data are shown as means ± SDs (n = 3). Data were analyzed by one-way ANOVA with post-hoc (Tukey). $^{**}p < 0.01$ and $^{***}p < 0.001$. hCdHs, human chemically derived hepatic progenitors; hPHs, human primary hepatocytes; PCL, polycaprolactone.

layer-by-layer manner, the printing paths were determined in three different sizes, thereby assembling the fabricated sheet scaffold, as shown in Fig. 2C. The use of a 3D printing system implies that the framework can be designed and tailor-made in a patient-specific manner with respect to the size or shape of lesions. For both electrospinning and 3D printing, we homogenously used an FDA-approved biomaterial PCL, which has a favorable mechanical flexibility (i.e., a rubber-like property owing to its low glass-transition temperature of −60 °C) that is suitable

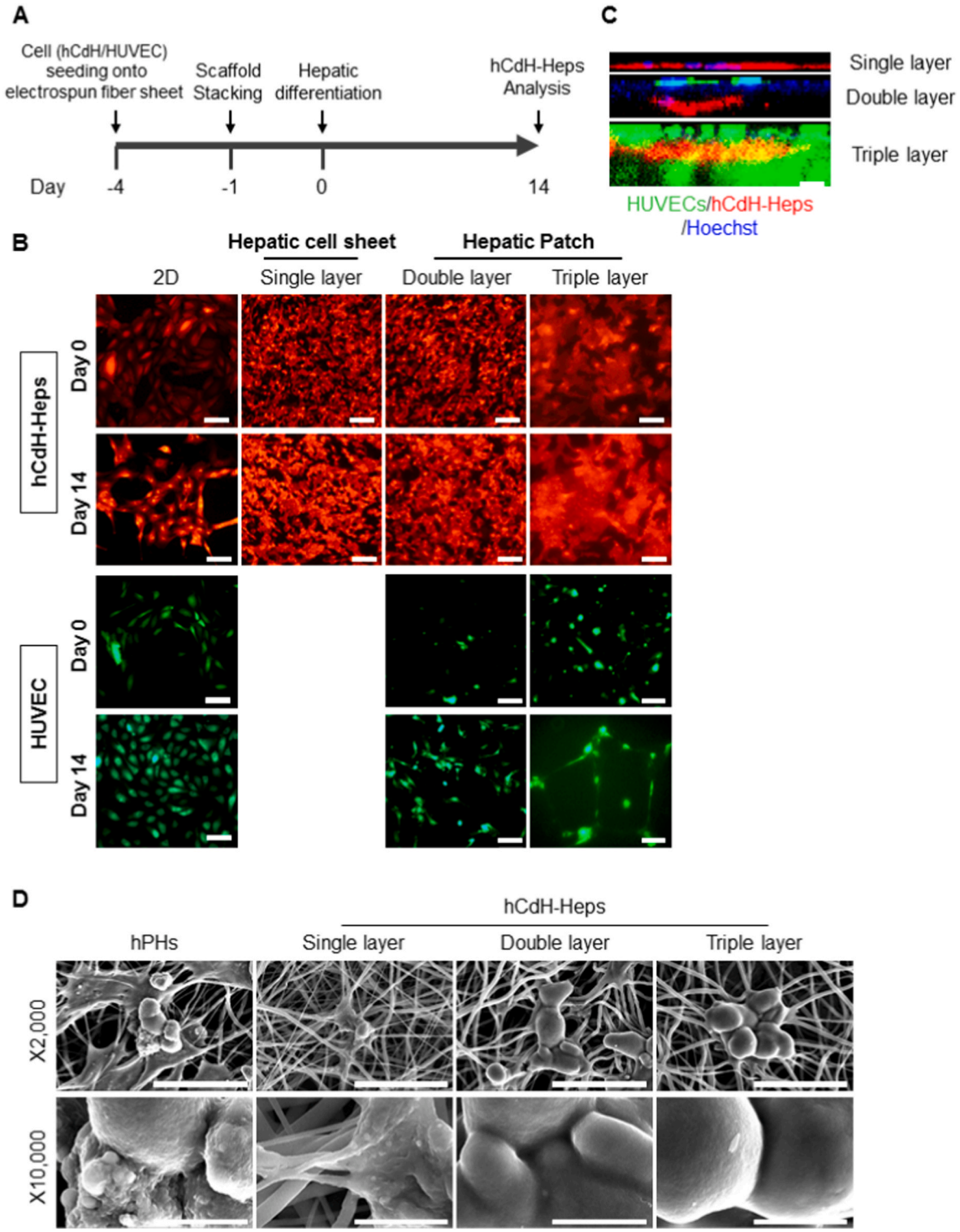

Fig. 3. Differentiation and morphological observations of hCdH-Heps on the hepatic cell sheet and patch. (A) Hepatic differentiation flow chart for hCdH-Heps on the electrospun fiber sheet. (B) Morphological changes of HUVECs and hCdH-Heps cultured on the electrospun fiber stacked sheets at days 0 and 14. The HUVECs and hCdH-Heps were labeled by GFP and mCherry, respectively. Scale bar, 100 μm. (C) Z-stacking of hepatic cell sheet and patch structures measured by a confocal microscope. Blue, Hoechst 33342; Green, HUVECs; hCdH-Heps, Red. Scale bar, 20 μm. (D) Scanning electron microscopy (SEM) image of hPHs and layered hCdH-Heps cultured on electrospun fiber sheets at day 14. Scale bars, 50 μm (× 2000) and 10 μm (× 10,000). hCdH-Heps, human chemically derived hepatic progenitors-derived hepatocytes; HUVECs, human umbilical vein endothelial cells; hPHs, human primary hepatocytes.

for soft tissue engineering. Owing to the good flexibility of the constituent materials, the overall multilayer assembly showed decent stability in the construction, which is an essential property for *in vivo* applications mentioned later in this article.

In previous studies using electrospun fiber scaffolds, cell functions tended to be more activated in scaffold mats with larger quantities of fibers, which ensured more effective topographical cues [40–44]. These results implied that the cultured cells preferentially interacted with multiple fibers, rather than with fewer fibers. Therefore, it is favorable to integrate a large number of fibers in the electrospun scaffold, i.e., the scaffold should have a high fiber density. In this context, we compared the differentiation capacities of hCdHs on different scaffolds with high and low densities of constituent fibers. The two types of scaffolds were prepared by electrospinning for 30 or 180 s, as shown in Fig. 2D. Considering cell perfusion can be obstructed in scaffolds with remarkably high fiber densities, the fiber density was restricted to a maximum spinning time of 180 s. Although mCherry-expressing hCdHs were differentiated on both types of electrospun sheets (Fig. 2E), the expression levels of hepatocyte-specific markers, including *ALB*, *ASGR1*, *HNF4A*, *MRP2*, *ATT*, and *CYP3A4*, were increased in the high-density scaffolds than in the low-density scaffolds (Fig. 2F). These results suggest that multiple fibers attached to cells provide favorable topographic effects of a 3D liver microanatomy and ultrastructure because they mimic the parenchymal space of the liver *in vivo*. Considering the hepatocyte size of 15–30 μm [45], the number of underlying fibers per area was estimated to be less than 10 fibers and several tens of fibers for the low- and high-density scaffolds, respectively. Therefore, a high-density sheet electrospun for 180 s was used in subsequent experiments to exploit the demonstrated hepatic functionality.

3.3. Fabrication of the hepatic patch by stacking the cell-laden electrospun fibrous sheets

To fabricate the hepatic patch, we seeded hCdHs and HUVECs onto each electrospun fibrous sheet and hierarchically stacked them individually 4 days before hepatic differentiation (Fig. 3A and Scheme 1). Because HUVECs develop in the early stage of embryogenesis [46], they are essential for organogenesis and cellular differentiation and secreting several growth factors called angiocrine factors, and increased VEGF expression in regenerating livers contributes to the proliferation of sinusoidal endothelial cells [47–49]. Previously, hepatocyte-like cells were cultured with HUVECs to generate liver buds. These liver buds were more similar to human liver tissue than the liver buds cultured without HUVECs [50]. Therefore, we generated a multilayered hepatic patch and performed hepatic differentiation for 14 days after stacking the electrospun fibrous layers (Fig. 3A). To facilitate observation, GFP and mCherry were used to tag HUVECs and hCdHs, respectively. On day 14, the HUVECs formed a tube shape in the triple-layered hepatic patch (HUVECs, hCdH-Heps, and HUVEC layers; Fig. 3B) and were slightly differentiated in the double layers (HUVECs and hCdH-Heps layers) without significant changes compared with their state before differentiation (Fig. 3B). When compared morphologically, the hCdH-Heps in the double- and triple-layered hepatic patches showed more aggregation than that in the 2D control. In addition, on observation of the z-stacking of the hepatic patch, HUVECs (green) and hCdH-Heps (red) were stacked in a layer-by-layer manner in the double- and triple-layered hepatic patches (Fig. 3C). To investigate the cell morphology and distribution of hCdH-Heps on each electrospun layer, we produced 3D surface images using SEM [51] for each of the hCdH-Heps layers (Fig. 3D). As expected, the hCdH-Heps were combined and showed a size similar to that of hPHs in the double- and triple-layered hepatic patches. These results showed that cell–cell interaction and desired cellular morphology were achieved using HUVECs in the double- and triple-layered hepatic patches.

3.4. Evaluation of the hepatic function of the layered hepatic patch in vitro

Next, we tested the marker expression of hCdH-Heps in the hepatic patch using RT-qPCR and immunostaining. The expression levels of hepatocyte-specific marker genes (*ALBUMIN*, *ASGR1*, *CK18*, *MRP2*, and *CYP3A4*) and proteins (ALBUMIN, HNF4α, and CK18) in hCdH-Heps were significantly elevated in the hepatic patch compared with those in the 2D culture (Fig. 4A and B). In the 2D culture, induction of hepatic differentiation with HUVECs (2D co-culture) increased the expression of hepatocyte-specific markers compared with that in the 2D culture without HUVECs (2D), but the hCdH-Heps differentiated on the hepatic patch showed a significantly increased hepatic marker expression compared with that in the 2D co-culture (Fig. 4A). Therefore, we used only the 2D culture as a control for further experiments to focus on the ability of the hepatic patch, rather than focusing on the functional ability of HUVECs. Next, to test the functional activity of the hepatic patch, the hepatic function was determined by measuring albumin secretion. As shown in Fig. 4C, albumin secretion by hCdH-Heps on the hepatic patch increased in a time-dependent manner. These results showed that the *in vivo*-like structure of the electrospun sheets increased the hepatic differentiation capacity of the hCdHs. In addition, an analysis of CYP activity, which is one of the functional features of hepatocytes, confirmed that CYP activity increased with the increase in number of layers (Fig. 4D). In particular, CYP1A2, CYP2C9, and CYP3A4 activity was significantly increased in the hepatic patch (Fig. 4D). CYP1A2 is localized in the endoplasmic reticulum and metabolizes xenobiotics in the body, such as polyunsaturated fatty acids, caffeine, aflatoxin Bi, and paracetamol (acetaminophen), into signaling molecules [52]. Moreover, the thickness of the differentiated hepatocytes was also increased (Fig. 4E). Hepatocyte thickness is one of the main factors regulating hepatic function. Large cells require increased mRNA, ribosome, and protein synthesis to maintain cellular function [53]. In addition to the internal events in cells, VEGF, HGF, and SDF-1, derived from surrounding cells and endothelial cells, regulate the redistribution of the cytoskeleton [54,55]. However, the influence of cell size on gene and protein expression remains unclear. These results indicated that the hepatic patch with endothelial cells not only induced morphological changes in hCdH-Heps but also exhibited mature hepatic functions.

3.5. Identification of cellular events of patient-specific hCdHs in the hepatic patch

For enhancing hepatic differentiation of hCdHs on electrospun fibrous scaffolds with endothelial cells, we focused on the downstream signaling of OSM, a member of the IL-6 cytokine family, on addition of exogenous OSM to differentiate the hCdHs into hepatocytes. OSM is known to play a critical role in the maturation of hepatocytes and their differentiation from fetal hepatocytes [56] and various stem cells [57, 58] *in vitro*. In western blotting, the time course analysis of 2D hCdHs for detecting OSM-mediated downstream molecules [59] including JAK/-STAT3, PI3K/AKT, and MAPK during hepatic differentiation showed increased phosphorylation of most downstream molecules, except JNK, in a time-dependent manner after OSM treatment (Figure S2). Based on the time course analysis, we examined the activation of signaling molecules on a hepatic cell sheet (single layer) or a hepatic patch (triple layer) on days 3 and 10 during hepatic differentiation. We found that the hepatic cell sheet promoted consistent phosphorylation of OSM-mediated downstream molecules, whereas the phosphorylation of AKT was selectively increased with the use of the hepatic patch (Fig. 5A). We further confirmed these differential activations of OSM-mediated downstream molecules between the hepatic sheet and patch by quantification of western blotting using densitometry (Fig. 5B). Although we also investigated the possibility of the presence of other relevant factors, such as the HGF signaling pathway, to regulate hepatic differentiation by qPCR, the expression of HGF and c-MET was not

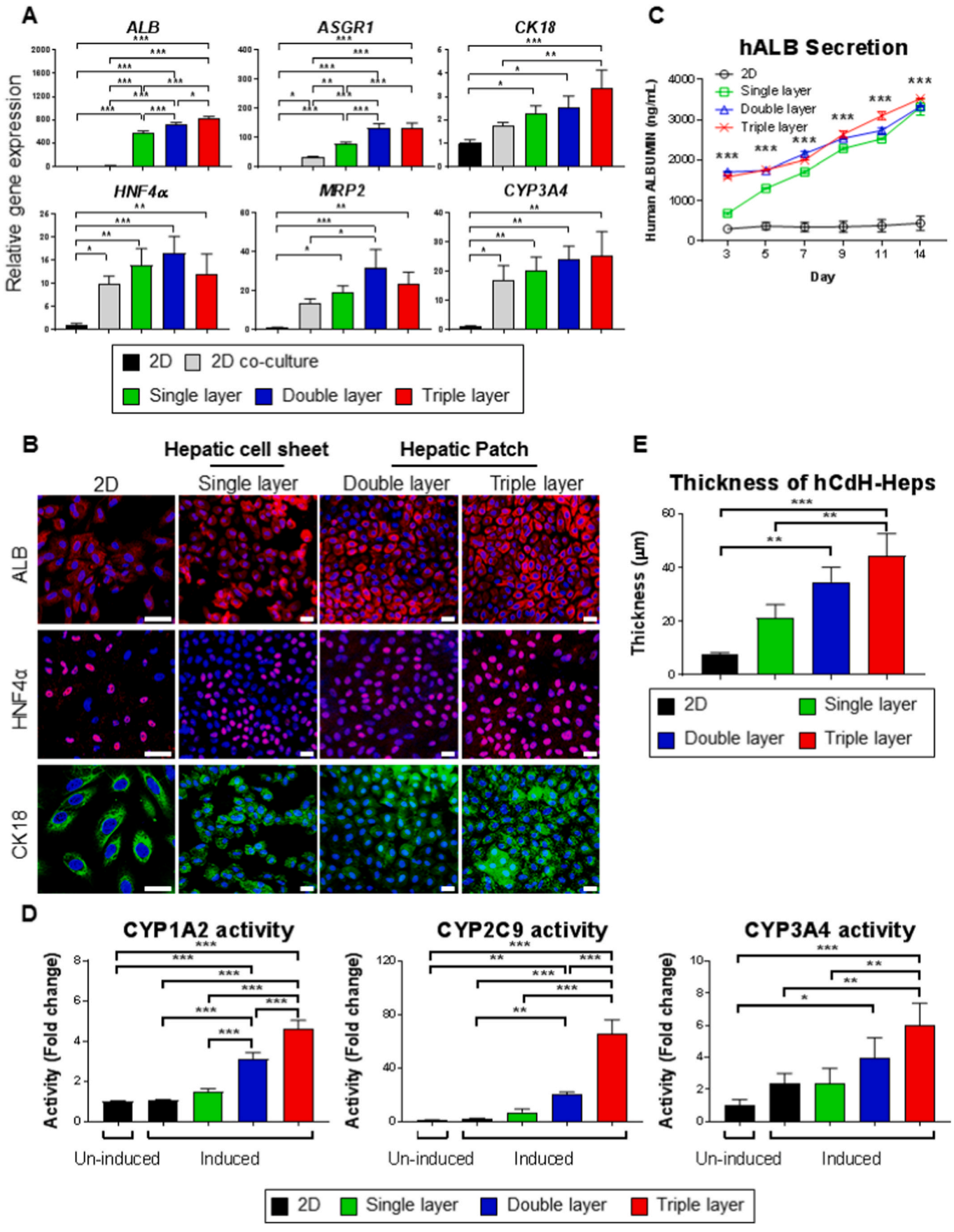

(caption on next page)

Fig. 4. Evaluation of the hepatic function *in vitro* in the hepatic cell sheet and patch. (A) Relative expression levels of mature hepatocyte-specific markers, like *ALB*, *ASGR1*, *HNF4α*, *CK18*, *MRP2*, and *CYP3A4* of the hCdH-Heps differentiated from hCdHs with 2D-cultured cells (black), 2D co-culture (grey), single (green), double (blue), and triple (red) layers, as measured by qRT-PCR. *GAPDH* was used as an internal control. Data are shown as the means ± SDs (n = 3). Data were analyzed by one-way ANOVA with post-hoc (Tukey). $*p < 0.05$, $**p < 0.01$, $***p < 0.001$. (B) hCdH-Heps differentiated from hCdHs on single, double, or triple layers of electrospun fiber stacked sheets expressed mature hepatocyte-specific markers, ALB (red, upper), HNF4α (red, middle), and CK18 (green, bottom). Nuclei were counterstained with Hoechst 33342 (blue). Scale bars, 50 μm. (C) The human albumin secretion levels (ng/mL) were measured in a conditioned hepatic differentiation medium. Each sample was harvested every couple of days. Data are means ± SDs (n = 3). Data were analyzed by one-way ANOVA with post-hoc (Tukey). $*p < 0.05$ and $**p < 0.01$. (D) Measurement of CYP1A2, CYP2C9 and CYP3A4 activity of the hCdH-Heps in the un-induced 2D culture and induced 2D culture, single-, double-, and triple-layered hepatic patch. CYP1A2 activity was induced by omeprazole and CYP2C9 and CYP3A4 activity were induced by rifampicin. Data are means ± SDs (n = 3). Data were analyzed by one-way ANOVA with post-hoc (Tukey). $*p < 0.05$, $**p < 0.01$ and $***p < 0.001$. (E) Thicknesses of hCdH-Heps on the 2D culture (black) and single- (green), double- (blue), and triple- (red) layered hepatic patch. In total, nine points from different areas were measured using Leica's LAS AF system. Data are shown as the means ± SDs. Data were analyzed by one-way ANOVA with post-hoc (Tukey). $**p < 0.01$ and $***p < 0.001$. hCdHs, human chemically derived hepatic progenitors; hCdH-Heps, hCdHs-derived hepatocytes.

affected by the use of the hepatic sheet or patch (data not shown), indicating that HGF signaling might not be associated with hepatic differentiation in terms of the impact of the hepatic sheet or patch. Interestingly, qPCR of both the OSM ligand and OSM-related receptors such as gq130, LIFR, and OSMR revealed significant upregulation of the OSM ligand gene (>3000 fold), but not of the OSM-related receptors, on the hepatic sheet and patch when compared with that in the 2D culture (Fig. 5C). These findings are supported by those of previous studies, which reported that the expression of growth factors and inflammatory cytokines, including IL-6, in various cells and *in vivo* can be modulated by fibrous scaffolds [17,18]. We further confirmed the enhanced protein expression and secretion of OSM using the hepatic sheet and patch after hepatic induction in comparison with those in the 2D culture, using western blotting and ELISA (Fig. 5D and E). Therefore, these results indicated that electrospun fibers might additionally activate OSM-mediated signaling pathways via the amplification of the OSM ligand to facilitate hepatic induction from hCdHs. In contrast, HUVECs may improve hepatic differentiation in an OSM-independent manner based on both the similar induction of OSM ligand by the electrospun fibers and the selective activation of AKT without changes in the electrospun fiber-activated OSM downstream signaling molecules, as shown in Fig. 5A–C. Communication between hepatocytes and endothelial cells may be mediated by VEGF and its tyrosine kinase receptor, VEGFR. Recently, $VEGFR2^{+}$ early hepatic progenitor cells in humans were reported to be capable of terminal differentiation into mature liver cell types [60]. Exogenous treatment of hepatic progenitor cells with VEGF results in a significant increase in hepatic genes such as *HNF4α*, *AFP*, and *ALBUMIN* [61]. Notably, in our study, VEGF secretion with the hepatic patch was more than two-fold higher than that with the hepatic sheet, as shown by ELISA (Fig. 5F). Considering the VEGF/VEGFR2 axis activates several downstream signaling pathways, including the PI3K/AKT pathway that trigger multiple biological responses in various cell types [62,63], it is likely that the significantly enhanced capacity for hepatic differentiation with the patch is associated with the VEGF produced by HUVECs (Fig. 5G).

3.6. Evaluation of therapeutic effects of hepatic patch on acute liver damage mouse model

Next, to determine whether the hepatic patch mitigates liver damage, we transplanted the hepatic patch (triple layer) into acute liver damage mouse models [64]. In this mouse model, liver damage can be induced by the administration of DT by controlling the human heparin-binding epidermal growth factor-like receptor (HB-EGF) with an albumin promoter [65]. Transplantation experiments were performed by carefully covering the surface of the damaged liver with the differentiated hepatic patch. After 1 week and 4 weeks, each mouse liver was harvested and embedded in paraffin for histological analysis (Fig. 6A). The hepatic patch was stably attached with the DT-treated liver, and it mitigated liver damage as compared to the DT-only control group (Fig. 6B). The DT-only group showed necrosis in the liver through DT-induced injury, but the group that received the hepatic patch transplant showed an undamaged histology (Figure S3A). After 4 weeks, it was concluded that the integration of the hepatic patch occurred after more than 1 week after transplantation, and interestingly, healthy morphology was observed even in the different lobes which were not uncovered by the hepatic patch at 4 weeks in the transplanted group. These results suggest that the therapeutic effect of the hepatic patch is not limited to the covered lobe, but it affects the entire liver. In addition, the DT-only group showed a high mortality rate, and all mice died before 7 weeks (Fig. 6C). However, the hepatic patch-transplanted group showed an increased survival rate of more than 70%. In addition, the expression levels of serum hepatic damage markers, including ALT, total bilirubin, and ALP, were significantly reduced and total albumin expression level was increased in the hepatic patch-transplanted group than 2D transplanted mice and negative control (Fig. 6D), indicating that the transplantation of the hepatic patch restored liver function. We further confirmed the engraftment of 2D-cultured hCdHs and the hepatic patch upon transplantation. Immunofluorescence staining showed that the hCdH-Heps on the hepatic patch stably expressed mature hepatic markers such as ALB, human ASGPR1, CK18, and HNF4A, as well as those of hCdHs alone after transplantation (Fig. 6E and S3B). Notably, the hepatic patch-transplanted group showed a significantly increased level of human albumin in mouse serum compared to that of the 2D-cultured hCdHs in a time-dependent manner after transplantation (Fig. 6F). Based on human albumin levels in mouse serum, we found similar results of human albumin secretion (>1000 ng/mL) in the hCdHs generated from liver tissue which were deived biopsy and surgical specimen [4]. Interestingly, a CD31-positive area, which is known to be a blood vessel marker, was observed with a vessel-like structure in the transplanted hepatic patch at 4 weeks. These data suggested that functional blood vessel-like structures might generate in the patch (Figure S3C). Human albumin secretion also significantly increased in the patch than in the 2D-cultured cells in a time-dependent manner after transplantation (Fig. 6F). Collectively, our data suggest that the hCdH-Heps cultured on the electrospun fiber stacked sheets can stably engraft in the host liver after transplantation and play a role similar to that of the original liver through the synthesized blood vessel-like structures.

Cell-based therapy has been developed as an alternative to liver transplantations and has traditionally been divided into autologous and allogeneic therapies. For clinical applications, at least 1×10^9 cells are needed [66]. Theoretically, 1×10^9 cells can be obtained from 1000 cells × 20 population doublings (1000 × 220 = 1,048,576,000 cells). Since the population doubling times of hCdHs is about 35 h, a duration of 700 h is needed for 20 population doublings. Therefore, after 29 days, we obtained 1×10^9 cells from 1000 cells. Using biomaterials combined with cell therapy and patient-specific hCdHs, we elucidated that the hepatic patch effectively repopulated damaged parenchyma and exhibited a high survival rate (>70%), along with the restoration of liver function, in a preclinical mouse model. These findings may contribute in improving the efficacy of stem cell transplantations and its clinical applications, especially in the case of autologous cell-based therapy for the treatment of acute liver failure. For allogeneic cell-based therapies in

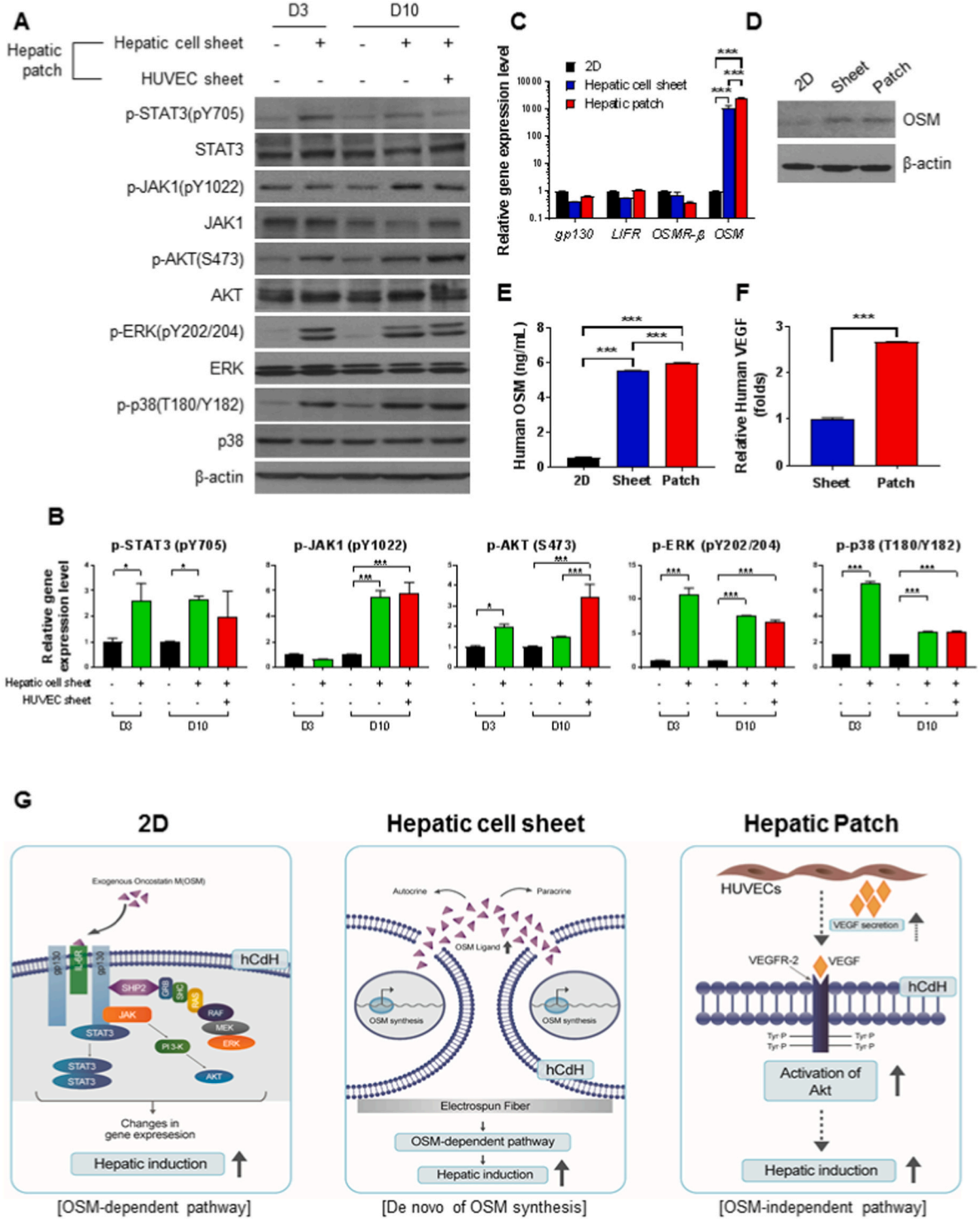

Fig. 5. Evaluation of cellular events of patient-specific hCdHs in the hepatic patch. The hCdHs were differentiated into hepatocytes in the hepatic cell sheet or hepatic patch under OSM treatment for hepatic induction with or without HUVECs. (A) Western blotting for pSTAT3, STAT3, pJAK1, JAK1, pAKT, AKT, pERK1/2, ERK1/2, pp38, and p38 with or without HUVECs. Beta-actin was used as a loading control. (B) Quantification of western blotting by densitometry. Data are shown as the means ± SDs. Data were analyzed by one-way ANOVA with post-hoc (Tukey). *$p < 0.05$ and ***$p < 0.001$. (C) RT-qPCR analysis of OSM-related receptors *gp130*, *LIFR*, and *OSMR*, and ligand *OSM* gene expression of hCdHs cultured in 2D cells (black), hepatic cell sheet (blue), and hepatic patch (red). *GAPDH* was used as an internal control. Data are shown as the means ± SDs and analyzed by two-way ANOVA with post-hoc (Tukey). ***$p < 0.001$. (D) Western blotting for OSM. Beta-actin was used as a loading control. The hCdHs were differentiated into hepatocytes after 10 days from either 2D hCdH cells or sheet or patch. (E, F) Human OSM or VEGF secretion levels (ng/mL) were measured in the conditioned hepatic differentiation medium, respectively. The sample was harvested on day 10 during hepatic differentiation. VEGF secretion level of the patch was calculated relative to that of the sheet. Data are means ± SDs (n = 3). Data were analyzed by one-way ANOVA with post-hoc (E) and two-tailed t-tests (F) (***$p < 0.001$). (G) The hypothesis of mechano-transduction signal pathways by electrospun fiber scaffolds in the hepatic patch system. OSM, oncostatin M; AKT, protein kinase B; hCdHs, human chemically derived hepatic progenitors; hCdH-Heps, hCdHs-derived hepatocytes; HUVECs, human umbilical vein endothelial cells; VEGF, vascular endothelial growth factor.

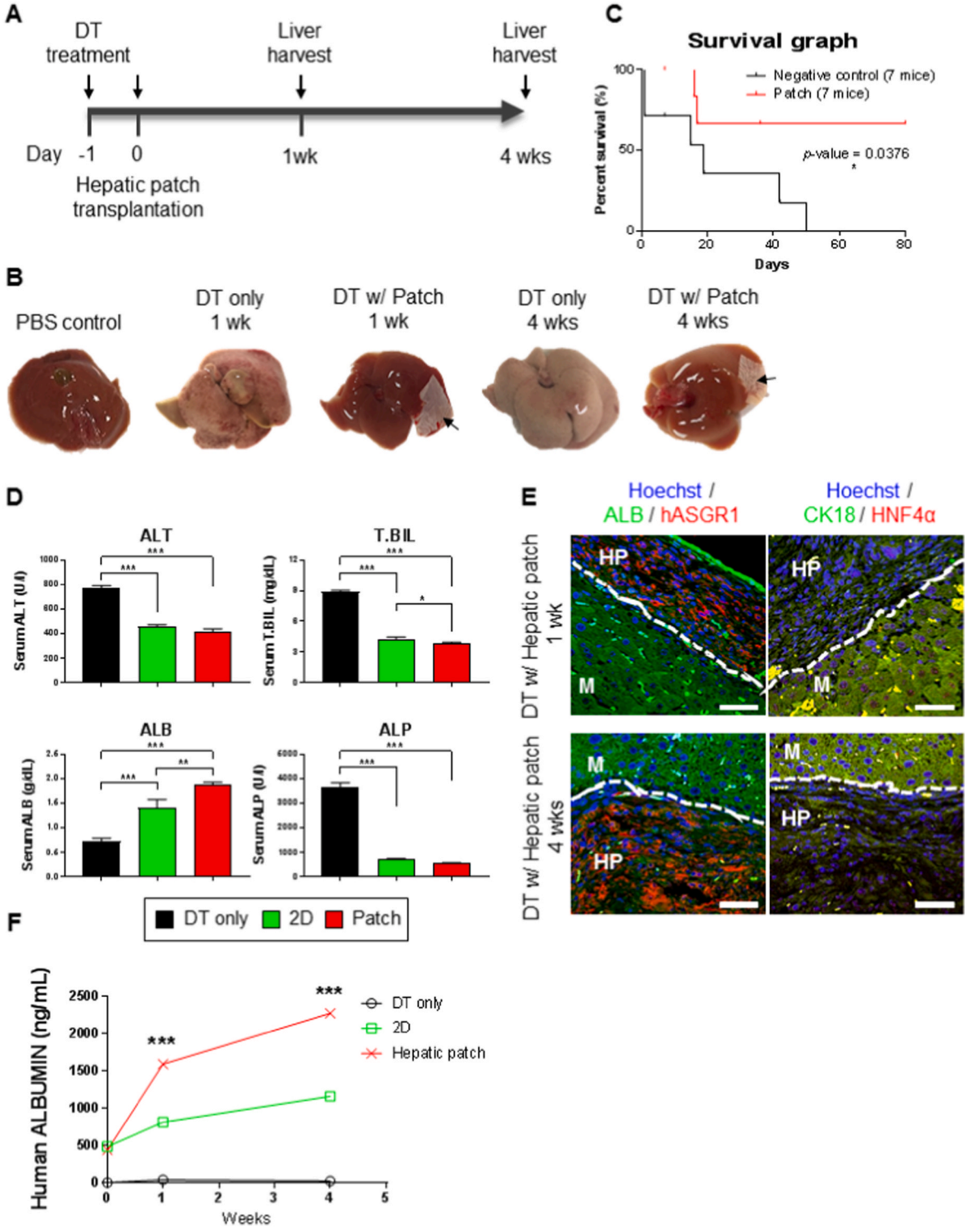

Fig. 6. Therapeutic potential of hepatic patch *in vivo*. (A) Schematic diagram for transplantation. Before one day of transplantation, DT was administered to mice. After 1 and 4 weeks, the transplanted hepatic patch was harvested for analysis. (B) Liver images taken from mouse models. Black arrow shows the transplanted hepatic patch. (C) Survival rate of the mice after transplantation with hepatic patch (n = 7) and the negative control group (n = 7). Survival analysis was analyzed as a Kaplan-Meier curve using GraphPad Prism 7. Log-rank test $p = 0.0376$. (D) Blood testing of liver-damaged mouse model: Aspartate aminotransferase (AST), alanine aminotransferase (ALT), total bilirubin (T.BIL), and albumin (ALB) in serum of 2D transplanted (n = 3), patch transplanted (n = 3) and negative control (n = 3) groups. Data are shown as the means ± SDs. Data were analyzed by one-way ANOVA with post-hoc (Tukey). $^{*}p < 0.05$, $^{**}p < 0.01$ and $^{***}p < 0.001$. (E) Immunostaining of the liver at 1 week and 4 weeks after transplantation of the hepatic patch. The hCdH-Heps on the hepatic patch were identified with ALBUMIN (green)/human ASGR1 (red) and CK18 (green)/HNF4α (red). Nuclei were counterstained with Hoechst 33342 (blue). Scale bars, 50 μm. M, mouse liver; HP, Hepatic patch. (F) Human albumin in mouse serum on 0, 1 and 4 weeks after hCdHs and hepatic patch transplantation. Mice injected DT only served as a negative control. Data analyzed by two-way ANOVA with post-hoc (Tukey). $^{***}p < 0.001$. DT, diphtheria toxin; hCdHs, human chemically derived hepatic progenitors; hCdH-Heps, hCdHs-derived hepatocytes.

clinical trials, MSCs have been used in clinical settings for the treatment of liver diseases due to their immunomodulatory and anti-inflammatory potential. In a clinical applications reported recently, it has been proposed that in a combination therapy of two different cell types, including MSCs for liver regeneration, the treatment with MSCs induced tolerance upon liver transplantation [67]. Therefore, the approach of the combination of an allogeneic hepatic patch with MSCs may be of interest as a novel strategy for liver regeneration in the future.

4. Conclusion

Our study reported an efficient regenerative therapeutic strategy involving a patient-specific hepatic patch with a similar structure to that observed *in vivo* developed by combining an electrospun fibrous sheet stacking technique with liver biopsy-derived hepatic progenitor cells. The hCdHs cultured on the electrospun fibrous sheets differentiated into highly functional mature hepatocyte-like cells, and the stacking concept recapitulated histological characteristics similar to those of a normal liver. Furthermore, these hepatic patches developed using hCdHs and HUVECs demonstrated the ability to exhibit not only functional features but also therapeutic effects in acute liver damage models. It may be more appropriate to use liver sinusoidal endothelial cells, hepatic stellate cells and Kupffer cells instead of HUVECs for increasing potential of clinical trials and *in vivo* mimicking. Therefore, our hepatic patch system provides a technique for the generation of artificial livers and may have potential clinical applications in the future.

Declaration of competing interest

The authors declare that they have no known competing financial interests or personal relationships that could have appeared to influence the work reported in this paper.

Acknowledgements

This research was supported by grants from the Medical Research Center (NRF-2017R1A5A2015395) and Basic Science Research Program (2019R1F1A1061148 and 2020R1I1A1A01070097) funded by the National Research Foundation of Korea Ministry of Science and ICT and by the research and funding of Hanyang University (HY-2020).

Appendix A. Supplementary data

Supplementary data to this article can be found online at https://doi.org/10.1016/j.biomaterials.2021.120899.

Credit author statement

Yohan Kim: Conduting main experiment, Writing manuscript. Young Won Kim: Fabrication of hepatic patch. Seung Bum Lee: Analysis of protein expression. Kyojin Kang: Human Liver Biopsy. Sangtae Yoon: Formal analysis. Jaemin Jeong: Writing- Reviewing and Editing. Suk-Hee Park: Writing- Reviewing and Editing. Dongho Choi: Writing-Reviewing and Editing.

Data availability

The raw/processed data in this study are available from the authors upon request.

References

[1] I.J. Fox, G.Q. Daley, S.A. Goldman, J. Huard, T.J. Kamp, M. Trucco, Stem cell therapy. Use of differentiated pluripotent stem cells as replacement therapy for treating disease, Science 345 (2014) 1247391.
[2] S.J. Yu, A concise review of updated guidelines regarding the management of hepatocellular carcinoma around the world: 2010-2016, Clin. Mol. Hepatol. 22 (2016) 7–17.
[3] S.H. Bae, [Clinical application of stem cells in liver diseases], Kor. J. Hepatol. 14 (2008) 309–317.
[4] Y. Kim, K. Kang, S.B. Lee, D. Seo, S. Yoon, S.J. Kim, et al., Small molecule-mediated reprogramming of human hepatocytes into bipotent progenitor cells, J. Hepatol. 70 (2019) 97–107.
[5] K. Ohashi, T. Yokoyama, M. Yamato, H. Kuge, H. Kanehiro, M. Tsutsumi, et al., Engineering functional two- and three-dimensional liver systems in vivo using hepatic tissue sheets, Nat. Med. 13 (2007) 880–885.
[6] A. da Silva Morais, S. Vieira, X. Zhao, Z. Mao, C. Gao, J.M. Oliveira, et al., Advanced biomaterials and processing methods for liver regeneration: state-of-the-art and future trends, Advanced healthcare materials 9 (2020), e1901435.
[7] Y. Nagamoto, K. Takayama, K. Ohashi, R. Okamoto, F. Sakurai, M. Tachibana, et al., Transplantation of a human iPSC-derived hepatocyte sheet increases survival in mice with acute liver failure, J. Hepatol. 64 (2016) 1068–1075.
[8] X. Ma, X. Qu, W. Zhu, Y.S. Li, S. Yuan, H. Zhang, et al., Deterministically patterned biomimetic human iPSC-derived hepatic model via rapid 3D bioprinting, Proc. Natl. Acad. Sci. U.S.A. 113 (2016) 2206–2211.
[9] N. Itaba, Y. Matsumi, K. Okinaka, A.A. Ashla, Y. Kono, M. Osaki, et al., Human mesenchymal stem cell-engineered hepatic cell sheets accelerate liver regeneration in mice, Sci. Rep. 5 (2015) 16169.
[10] E.S. Mirdamadi, D. Kalhori, N. Zakeri, N. Azarpira, M. Solati-Hashjin, Liver tissue engineering as an emerging alternative for liver disease treatment. Tissue engineering Part B, Review 26 (2020) 145–163.
[11] B. Dhandayuthapani, Y. Yoshida, T. Maekawa, D.S. Kumar, Polymeric scaffolds in tissue engineering application: a review, International Journal of Polymer Science (2011).
[12] N. Bhardwaj, S.C. Kundu, Electrospinning: a fascinating fiber fabrication technique, Biotechnol. Adv. 28 (2010) 325–347.
[13] M.S. Kim, B. Lee, H.N. Kim, S. Bang, H.S. Yang, S.M. Kang, et al., 3D tissue formation by stacking detachable cell sheets formed on nanofiber mesh, Biofabrication 9 (2017), 015029.
[14] U.H. Ko, S. Park, H. Bang, M. Kim, H. Shin, J.H. Shin, Promotion of myogenic maturation by timely application of electric field along the topographical alignment, Tissue Eng. 24 (2018) 752–760.
[15] M.T. Levy, M. Trojanowska, A. Reuben, Oncostatin M: a cytokine upregulated in human cirrhosis, increases collagen production by human hepatic stellate cells, J. Hepatol. 32 (2000) 218–226.
[16] A. Miyajima, T. Kinoshita, M. Tanaka, A. Kamiya, Y. Mukouyama, T. Hara, Role of Oncostatin M in hematopoiesis and liver development, Cytokine Growth Factor Rev. 11 (2000) 177–183.
[17] E. Saino, M.L. Focarete, C. Gualandi, E. Emanuele, A.I. Cornaglia, M. Imbriani, et al., Effect of electrospun fiber diameter and alignment on macrophage activation and secretion of proinflammatory cytokines and chemokines, Biomacromolecules 12 (2011) 1900–1911.
[18] G. Ramanathan, T. Muthukumar, U. Tirichurapalli Sivagnanam, In vivo efficiency of the collagen coated nanofibrous scaffold and their effect on growth factors and pro-inflammatory cytokines in wound healing, Eur. J. Pharmacol. 814 (2017) 45–55.
[19] F.W. Vondran, E. Katenz, R. Schwartlander, M.H. Morgul, N. Raschzok, X. Gong, et al., Isolation of primary human hepatocytes after partial hepatectomy: criteria for identification of the most promising liver specimen, Artif. Organs 32 (2008) 205–213.
[20] L. Shor, S. Guceri, X. Wen, M. Gandhi, W. Sun, Fabrication of three-dimensional polycaprolactone/hydroxyapatite tissue scaffolds and osteoblast-scaffold interactions in vitro, Biomaterials 28 (2007) 5291–5297.
[21] L. Rambhatla, C.P. Chiu, P. Kundu, Y. Peng, M.K. Carpenter, Generation of hepatocyte-like cells from human embryonic stem cells, Cell Transplant. 12 (2003) 1–11.
[22] H. Basma, A. Soto-Gutierrez, G.R. Yannam, L. Liu, R. Ito, T. Yamamoto, et al., Differentiation and transplantation of human embryonic stem cell-derived hepatocytes, Gastroenterology 136 (2009) 990–999.
[23] G.J. Sullivan, D.C. Hay, I.H. Park, J. Fletcher, Z. Hannoun, C.M. Payne, et al., Generation of functional human hepatic endoderm from human induced pluripotent stem cells, Hepatology 51 (2010) 329–335.
[24] Y.F. Chen, C.Y. Tseng, H.W. Wang, H.C. Kuo, V.W. Yang, O.K. Lee, Rapid generation of mature hepatocyte-like cells from human induced pluripotent stem cells by an efficient three-step protocol, Hepatology 55 (2012) 1193–1203.
[25] K.D. Lee, T.K. Kuo, J. Whang-Peng, Y.F. Chung, C.T. Lin, S.H. Chou, et al., In vitro hepatic differentiation of human mesenchymal stem cells, Hepatology 40 (2004) 1275–1284.
[26] A. Banas, T. Teratani, Y. Yamamoto, M. Tokuhara, F. Takeshita, G. Quinn, et al., Adipose tissue-derived mesenchymal stem cells as a source of human hepatocytes, Hepatology 46 (2007) 219–228.
[27] S. Sekiya, A. Suzuki, Direct conversion of mouse fibroblasts to hepatocyte-like cells by defined factors, Nature 475 (2011) 390–393.
[28] P. Huang, L. Zhang, Y. Gao, Z. He, D. Yao, Z. Wu, et al., Direct reprogramming of human fibroblasts to functional and expandable hepatocytes, Cell stem cell 14 (2014) 370–384.
[29] D.G. Zacharias, T.J. Nelson, P.S. Mueller, C.C. Hook, The science and ethics of induced pluripotency: what will become of embryonic stem cells? Mayo Clin. Proc. 86 (2011) 634–640.

[30] M. Buehr, J. Nichols, F. Stenhouse, P. Mountford, C.J. Greenhalgh, S. Kantachuvesiri, et al., Rapid loss of Oct-4 and pluripotency in cultured rodent blastocysts and derivative cell lines, Biol. Reprod. 68 (2003) 222–229.
[31] L. Barkholt, E. Flory, V. Jekerle, S. Lucas-Samuel, P. Ahnert, L. Bisset, et al., Risk of tumorigenicity in mesenchymal stromal cell-based therapies–bridging scientific observations and regulatory viewpoints, Cytotherapy 15 (2013) 753–759.
[32] A.S. Lee, C. Tang, M.S. Rao, I.L. Weissman, J.C. Wu, Tumorigenicity as a clinical hurdle for pluripotent stem cell therapies, Nat. Med. 19 (2013) 998–1004.
[33] P. Thampanitchawong, T. Piratvisuth, Liver biopsy:complications and risk factors, World J. Gastroenterol. 5 (1999) 301–304.
[34] S. Agarwal, J.H. Wendorff, A. Greiner, Progress in the field of electrospinning for tissue engineering applications, Adv. Mater. 21 (2009) 3343–3351.
[35] S. Nemati, S.J. Kim, Y.M. Shin, H. Shin, Current progress in application of polymeric nanofibers to tissue engineering, Nano convergence 6 (2019) 36.
[36] Z. Liu, S. Ramakrishna, X. Liu, Electrospinning and emerging healthcare and medicine possibilities, APL bioengineering 4 (2020), 030901.
[37] G. Mazza, K. Rombouts, A. Rennie Hall, L. Urbani, T. Vinh Luong, W. Al-Akkad, et al., Decellularized human liver as a natural 3D-scaffold for liver bioengineering and transplantation, Sci. Rep. 5 (2015) 13079.
[38] M.D. Shoulders, R.T. Raines, Collagen structure and stability, Annu. Rev. Biochem. 78 (2009) 929–958.
[39] M. Li, M.J. Mondrinos, M.R. Gandhi, F.K. Ko, A.S. Weiss, P.I. Lelkes, Electrospun protein fibers as matrices for tissue engineering, Biomaterials 26 (2005) 5999–6008.
[40] S.H. Park, J.W. Hong, J.H. Shin, D.Y. Yang, Y. Yang, Quantitatively controlled fabrication of uniaxially aligned nanofibrous scaffold for cell adhesion, J. Nanomater. (2011).
[41] D. Phu, L.S. Wray, R.V. Warren, R.C. Haskell, E.J. Orwin, Effect of substrate composition and alignment on corneal cell phenotype, Tissue Eng. 17 (2011) 799–807.
[42] S.H. Park, M.S. Kim, B. Lee, J.H. Park, H.J. Lee, N.K. Lee, et al., Creation of a hybrid scaffold with dual configuration of aligned and random electrospun fibers, ACS Appl. Mater. Interfaces 8 (2016) 2826–2832.
[43] K. Wang, L. Liu, J. Xie, L. Shen, J. Tao, J. Zhu, Facile strategy to generate aligned polymer nanofibers: effects on cell adhesion, ACS Appl. Mater. Interfaces 10 (2018) 1566–1574.
[44] Y. Xu, G. Shi, J. Tang, R. Cheng, X. Shen, Y. Gu, et al., ECM-inspired micro/nanofibers for modulating cell function and tissue generation, Science advances 6 (2020).
[45] G. Mazza, W. Al-Akkad, A. Telese, L. Longato, L. Urbani, B. Robinson, et al., Rapid production of human liver scaffolds for functional tissue engineering by high shear stress oscillation-decellularization, Sci. Rep. 7 (2017) 5534.
[46] G. Pettinato, S. Lehoux, R. Ramanathan, M.M. Salem, L.X. He, O. Muse, et al., Generation of fully functional hepatocyte-like organoids from human induced pluripotent stem cells mixed with Endothelial Cells, Sci. Rep. 9 (2019) 8920.
[47] K. Matsumoto, H. Yoshitomi, J. Rossant, K.S. Zaret, Liver organogenesis promoted by endothelial cells prior to vascular function, Science 294 (2001) 559–563.
[48] E. Lammert, O. Cleaver, D. Melton, Induction of pancreatic differentiation by signals from blood vessels, Science 294 (2001) 564–567.
[49] D.J. Nolan, M. Ginsberg, E. Israely, B. Palikuqi, M.G. Poulos, D. James, et al., Molecular signatures of tissue-specific microvascular endothelial cell heterogeneity in organ maintenance and regeneration, Dev. Cell 26 (2013) 204–219.
[50] T. Takebe, K. Sekine, M. Enomura, H. Koike, M. Kimura, T. Ogaeri, et al., Vascularized and functional human liver from an iPSC-derived organ bud transplant, Nature 499 (2013) 481–484.
[51] S.D. Russell, C.P. Daghlian, Scanning electron-microscopic observations on de-embedded biological tissue-sections - comparison of different fixatives and embedding materials, J. Electron. Microsc. Tech. 2 (1985) 489–495.
[52] D.R. Nelson, D.C. Zeldin, S.M. Hoffman, L.J. Maltais, H.M. Wain, D.W. Nebert, Comparison of cytochrome P450 (CYP) genes from the mouse and human genomes, including nomenclature recommendations for genes, pseudogenes and alternative-splice variants, Pharmacogenetics 14 (2004) 1–18.
[53] S. Marguerat, J. Bahler, Coordinating genome expression with cell size, Trends Genet. : TIG (Trends Genet.) 28 (2012) 560–565.
[54] T.X. Ngo, E. Nagamori, T. Kikuchi, T. Shimizu, T. Okano, M. Taya, et al., Endothelial cell behavior inside myoblast sheets with different thickness, Biotechnol. Lett. 35 (2013) 1001–1008.
[55] K. Kim, R. Utoh, K. Ohashi, T. Kikuchi, T. Okano, Fabrication of functional 3D hepatic tissues with polarized hepatocytes by stacking endothelial cell sheets in vitro, Journal of tissue engineering and regenerative medicine 11 (2017) 2071–2080.
[56] A. Kamiya, T. Kinoshita, Y. Ito, T. Matsui, Y. Morikawa, E. Senba, et al., Fetal liver development requires a paracrine action of oncostatin M through the gp130 signal transducer, EMBO J. 18 (1999) 2127–2136.
[57] D.C. Hay, D. Zhao, J. Fletcher, Z.A. Hewitt, D. McLean, A. Urruticoechea-Uriguen, et al., Efficient differentiation of hepatocytes from human embryonic stem cells exhibiting markers recapitulating liver development in vivo, Stem Cell. 26 (2008) 894–902.
[58] K. Si-Tayeb, F.K. Noto, M. Nagaoka, J. Li, M.A. Battle, C. Duris, et al., Highly efficient generation of human hepatocyte-like cells from induced pluripotent stem cells, Hepatology 51 (2010) 297–305.
[59] G. Dey, A. Radhakrishnan, N. Syed, J.K. Thomas, A. Nadig, K. Srikumar, et al., Signaling network of Oncostatin M pathway, Journal of cell communication and signaling 7 (2013) 103–108.
[60] O. Goldman, S. Han, M. Sourisseau, N. Dziedzic, W. Hamou, B. Corneo, et al., KDR identifies a conserved human and murine hepatic progenitor and instructs early liver development, Cell stem cell 12 (2013) 748–760.
[61] A.S. Arterbery, C.W. Bogue, Hhex is necessary for the hepatic differentiation of mouse ES cells and acts via vegf signaling, PloS One 11 (2016), e0146806.
[62] C.S. Abhinand, R. Raju, S.J. Soumya, P.S. Arya, P.R. Sudhakaran, VEGF-A/VEGFR2 signaling network in endothelial cells relevant to angiogenesis, Journal of cell communication and signaling 10 (2016) 347–354.
[63] H. Hu, S. Li, J. Li, C. Huang, F. Zhou, L. Zhao, et al., Knockdown of fibromodulin inhibits proliferation and migration of RPE cell via the VEGFR2-AKT pathway, Journal of ophthalmology (2018) 5708537.
[64] R.R. Zhang, Y.W. Zheng, B. Li, Y.Z. Nie, Y. Ueno, T. Tsuchida, et al., Hepatic stem cells with self-renewal and liver repopulation potential are harbored in CDCP1-positive subpopulations of human fetal liver cells, Stem Cell Res. Ther. 9 (2018) 29.
[65] M. Saito, T. Iwawaki, C. Taya, H. Yonekawa, M. Noda, Y. Inui, et al., Diphtheria toxin receptor-mediated conditional and targeted cell ablation in transgenic mice, Nat. Biotechnol. 19 (2001) 746–750.
[66] A. Dhawan, Clinical human hepatocyte transplantation: current status and challenges. Liver transplantation : official publication of the American Association for the Study of Liver Diseases and the, International Liver Transplantation Society 21 (Suppl 1) (2015) S39–S44.
[67] T. Squillaro, G. Peluso, U. Galderisi, Clinical trials with mesenchymal stem cells: an update, Cell Transplant. 25 (2016) 829–848.